Synthesis and characterization of LiMnPO$_4$ material as cathode for Li-ion batteries by a precipitation method and solid-state blending

R. El khalfaouy [a], H. El knidri, R. Belaabed, A. Addaou, A. Laajeb, A. Lahsini

Catalysis, Materials and Environment Laboratory, Sidi Mohamed Ben Abdellah University, Fez, Morocco

[a] *Corresponding Author. E-mail: redouan.elkhalfaouy@usmba.ac.ma; Tel: (+212610592650)*

Abstract

The phospho-olivine material LiMnPO$_4$ nanocrystal was identified as a promising cathode material for next generation Lithium-ion batteries and have been successfully synthesized by a fast method that brings together the precipitation technique and solid-state blending with MnCl$_2$.4H$_2$O , (NH$_4$)$_2$HPO$_4$ and LiCl as raw materials. The effect of the starting precursors (Mn, PO$_4$) concentration according to the calcination temperature (400 – 700°C) is discussed. The Variation of the synthetic parameters leads to LiMnPO$_4$ at 400°C when we work with equal reactant concentration and at 700°C when we use an excess of (NH$_4$)$_2$HPO$_4$ relatively to MnCl$_2$.4H$_2$O. The phase purity and composition were verified by X-ray diffraction (XRD) analysis, and the structure/morphology were observed by transmission electron microscopy (TEM) , scanning electron microscope (SEM), Fourier transform infrared (FT-IR) spectroscopy, Energy Dispersive X-ray analysis (EDS), Raman spectra. The general investigation demonstrates that there is a correlation among precursors concentration, calcinations temperature, crystal structure and morphology that can be exploited for the design of next generation lithium-ion batteries.

Keywords: Lithium-ion, synthesis, olivine, cathode, precipitation.

1. Introduction

the production and the storage of new and clean energies, are one of the future big challenges to mitigate on the one hand the exhaustion of the natural resources and in addition with the increasing use of systems requesting a contribution of electrical energy (portable electronic devices: microcomputers, telephones, video cameras, electric vehicles and hybrid,…). These various markets required the development of various electrochemical systems like the combustible batteries, the supercondensateurs and of course the batteries.

Since 1970 phospho-olivine structure became one of the potential cathode materials for Li-ion batteries [1-4]. In particular, Lithium manganese phosphate LiMnPO$_4$ and Lithium iron phosphate LiFePO$_4$ which are the most researched among these compounds possesses inherent chemical stability and thus improved safety, compared to the classical transition-metal oxide cathode materials.

Since the pioneering study on LiFePO$_4$ by Padhi et al. [5], significant efforts have been made to improve this material. [6-14]. But until now a series of lithium transition metal phosphates with an ordered olivine structure LiMPO$_4$ (M = Fe, Mn, Co, Ni …) have recently been investigated as attractive cathode materials because of their nontoxic, environment friendly and excellent thermal stability. Therefore, many research groups have focused their efforts on new synthetic methods for the preparation of olivine phosphates specially LiMnPO$_4$ and LiFePO$_4$ to improve their performances.

The advantages of LiMnPO$_4$ makes it one of the very promising cathode materials, the obvious one is its redox potential (4.1 V vs Li$^+$/Li), which is 0.7 V higher than that of LiFePO$_4$ but still within the typical electrolyte stability window. However, the kinetic of LiMnPO$_4$ is unusually sluggish, possibly due to the intrinsically low ionic and electronic conductivity and the interfacial strain between the lithiated and delithiated phase [15-17].

These limitations could be overcome by the use of very small particles (to increase the ionic conductivity) [29], embedded in a conductive matrix of Carbone (to increase the electronic conductivity) [30].

The synthesis of controlled size and morphology lithium-compounds is a key to solve the low ionic conductivity mentioned above. The process is very difficult due to their multi-component and complex structural chemistry. Until now, few general methods have been reported to prepare a pure phase of $LiMnPO_4$ nanocristals, among them the direct precipitation of $LiMnPO_4$ [18, 19], the sol−gel synthesis [20, 21], the polyol synthesis [22, 23], ceramic synthesis [24, 25], the ionothermal synthesis [26], the spray pyrolysis followed by wet- ball milling [27]. Whereas the low-temperature treatments typically lead to small and uniform active [18, 22, 25].

For all these reasons we successfully synthesized $LiMnPO_4$ using a modified method from the literature [28]; that brings together the precipitation technique and solid-state blending. We focused this work on the effect of raw material concentration as one of the major parameters to optimize.

2. Materials and methods

2.1. Preparation

In order to improve the raw material concentration effect, $LiMnPO_4$ was prepared in Two-Steps with two different concentrations.

In the first step (Table 1), a homogeneous mixture of reactants without lithium was prepared by stirring 0.5 M solution of $MnCl_2.4H_2O$ (99%, Riedel-dehaën) with an excess saturated ≈ 10 M of $(NH_4)_2HPO_4$ solution (99%, Merck) (the product called P1), and we prepared another product in which we used the same concentration (≈ 5M) for the both precursors $MnCl_2.4H_2O$ and $(NH_4)_2HPO_4$ (the product called P2). The resulting precipitate was aged at $90 \pm 5°C$ for 1 h, after that the product was filtered, washed with DI water several times and dried in a desiccator.

Table 1: Details about different conditions for preparing $MnPO_4·H_2O$ with precipitation method (the first step)

Precursors & parameters	$MnCl_2.4H_2O$	$(NH_4)_2HPO_4$	Preparation temperature	Stirring time	Final product
Protocol 1	0.5 M	≈ 10 M	$90 \pm 5°C$	1h	P1
Protocol 2	≈ 5M	≈ 5M	$90 \pm 5°C$	1h	P2

In the second step (Table 2), the composites from the first step were mixed with an adequate quantity of LiCl (99%, Riedel-dehaën) Using planetary ball milling (Pulversette-Fritsch) for 10 min at 300 rpm. The final $LiMnPO_4$ products were divided into two parts each one, and were calcined for 2 h in alumina crucibles at 400 and 700 °C.

Table 2: Details about different conditions for preparing $LiMnPO_4$ with solid-state blending (the second step)

Precursors & parameters	P1	P2	LiCl	Milling time	rpm	Calcination temperature	Final product
Protocol 1	0.918g	---------	0.201g	10 min	300	400 °C	Amorphous
						700 °C	$LiMnPO_4$
Protocol 2	--------	5.912g	1.351g	10 min	300	400 °C	$LiMnPO_4$
						700 °C	$LiMnPO_4$, Mn_3O_4, $Mn_3(PO_4)_2$

In order to prepare LiMnPO$_4$ doped by carbon source to get LiMnPO$_4$/C, a stoichiometric amount of LiMnPO$_4$ and Starch (Loba Chemie) were dispersed in ethanol solvent. The mixture was ball milled thoroughly in a planetary ball milling (Pulversette-Fritsch) with zirconia balls at room temperature for 10 min at 300 rpm. The mixture was then calcined at 400°C for the product P2 (called Product-2/C), and at 700°C for the product P1 (called Product-1/C), for 2 h in Air atmosphere. After cooling in furnace, the final black powders (LiMnPO$_4$/C) were obtained.
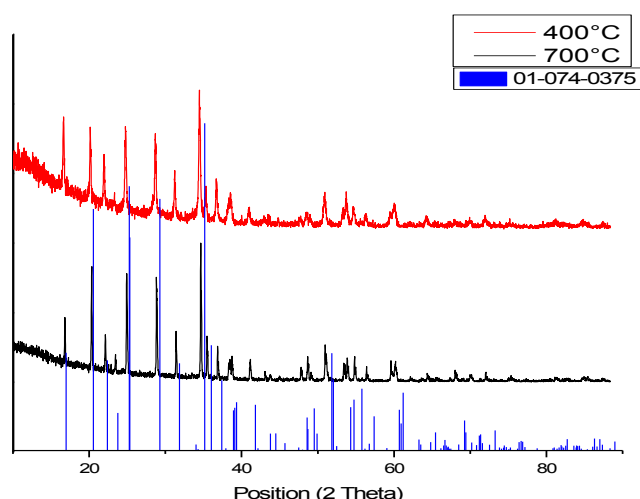
2.2. Characterization

The diffractometer of x-rays used is X' PERT PRO PANALATYCAl equipped with a detector with scintillation X' Celerator Ultrarapide with Beam of radiation Kα (λ = 0,154060 Nm), functioning with the tension 40 Kv and current 30 mA with a copper target was used to identify the crystalline phase of the materials. The surface morphology and the chemical compositions were observed with a scanning electron microscope with sweeping (FEI QUANTA 200) equipped with EDS for microanalysis of surface. The surface layer was observed with a transmission electron microscope FEI TECNAI G2 functioning with a resolution of 0.35 nm, a voltage of 120 KV and a magnification of 150 to 500,000 times". FTIR absorption spectra and Raman spectra of the as prepared materials were recorded by a VERTEX 70 de Bruker Optic spectrophotometer and a SENTARA de Bruker Optic respectively.

3. Results and discussion

3.1. X-ray diffraction (XRD)

All detectable peaks of the calcined product-1 at 700°C and 400 °C are shown in Fig. 1, the peaks at 700°C are indexed as LiMnPO$_4$ crystal structures according to the standard data PDF # 074-0375. However, no corresponding PDF standard files for the calcined product at 400 °C, which is indexed as an amorphous structure. The XRD patterns of the calcined product-2 at 700°C and 400 °C are shown in Fig. 2, while the peaks at 700°C are indexed as LiMnPO$_4$ crystal structure (with a trace impurity of Mn$_3$O$_4$ and Mn$_3$(PO$_4$)$_2$). In addition, all detectable peaks at 400 °C are indexed as LiMnPO$_4$ structure, which is identified using the standard data PDF # 033-0803. The obtained results indicate that these two compounds (Product-1 at 700°C and Product-2 at 400°C) crystallize in orthorhombic system with the space group Pmnb.
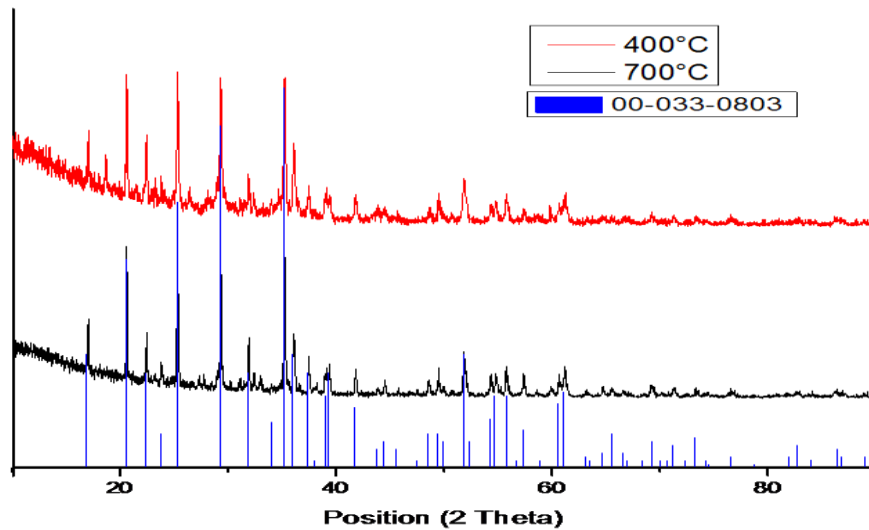

Figure 1 : XRD patterns of Product-1 synthesized at 400°C and at 700°C

3.2. Scanning electron microscope (SEM)

The varied morphology of as-prepared LiMnPO$_4$ and LiMnPO$_4$/C samples synthesized at different conditions (Product-1, Product-2) are shown in Fig. 3 and Fig. 4. From the SEM images it can be observed that all samples
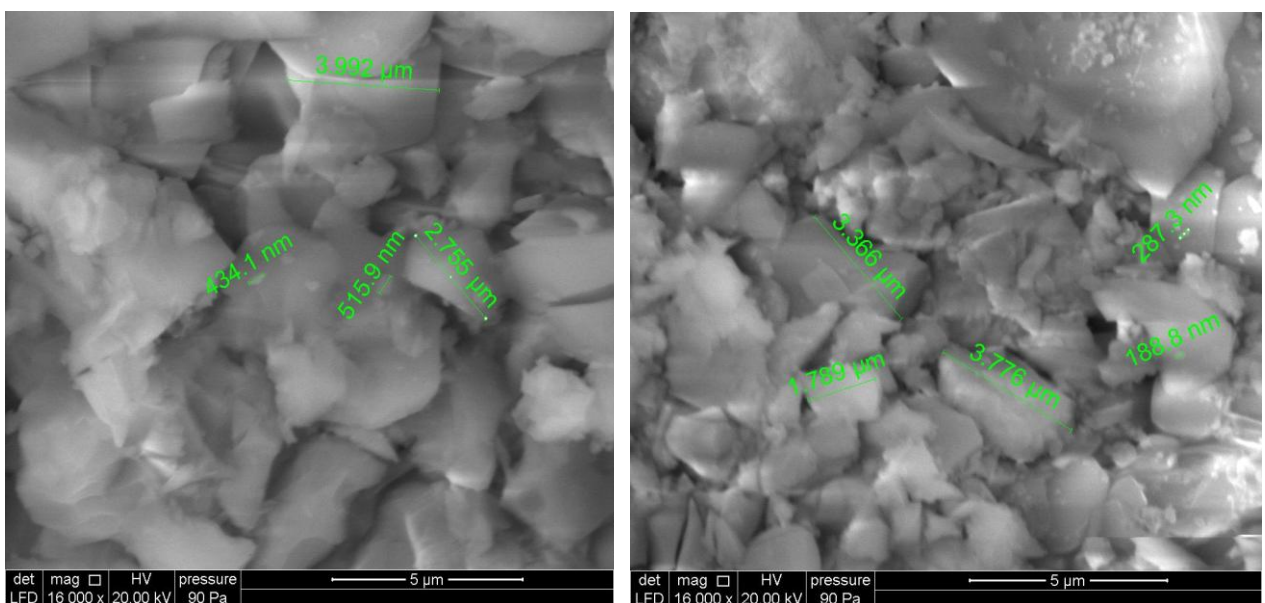
consist of secondary particles which are random in shape. These secondary particles are formed by loose aggregation of primary particles which also have different shapes. It proved that the chemical precipitation process, and the ball milling technique, can strongly effect the crystal growth and the final morphology.

The figure 3 (left) shows the SEM image of pure Product-1(at 700°C) with high agglomeration, the results shown a non-uniform distribution of the particles with a size between ~ 400 and 4000 nm. Figure 3 (right) shows SEM image of the carbon coated product Prodcut-1/C, it can be seen that the size of this product was reduced and it found to be between ~ 200 and 4000 nm.
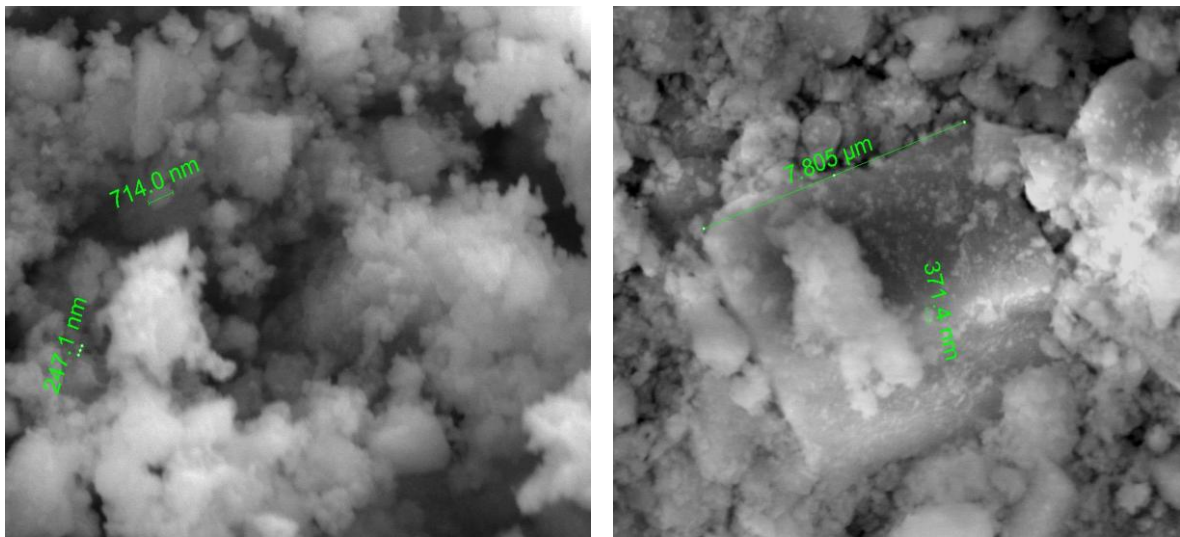

Figure 2 : XRD patterns of Product-2 synthesized at 400°C and at 700°C

The SEM image of the pure Product-2 (at 400°C) nanoparticles shown in figure 4 (left) show the agglomerated spherical shape and the particle size was found to be between ~200 and 800 nm. Figure 4 (right) show the SEM image of the carbon coated product Product-2/C nanoparticles, it show highly agglomeration and the appearance of a big particles size that is found to be ~ 8000 nm.
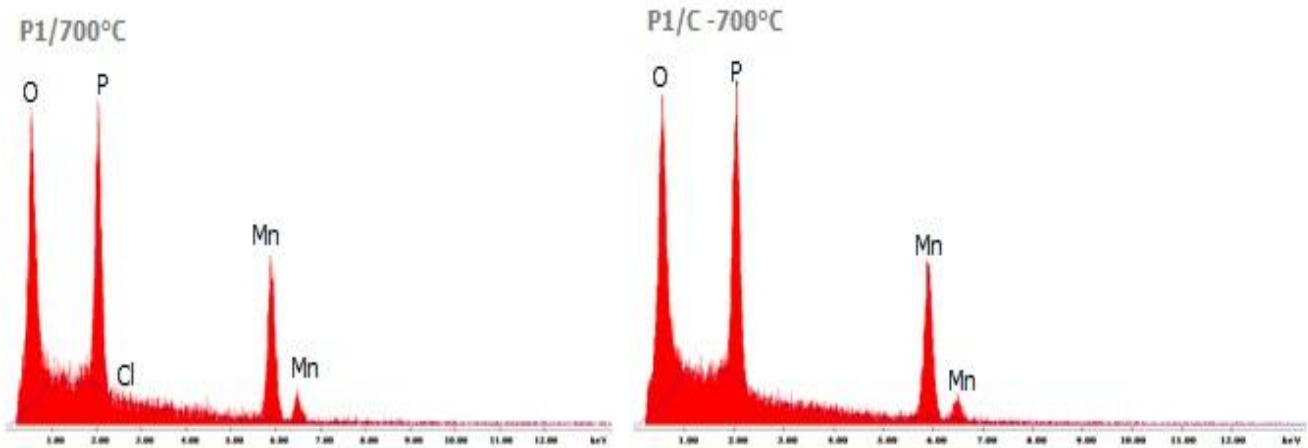

Figure 3 : SEM micrographs of the Product-1 (left) and Product-1/C (right) at 700°C
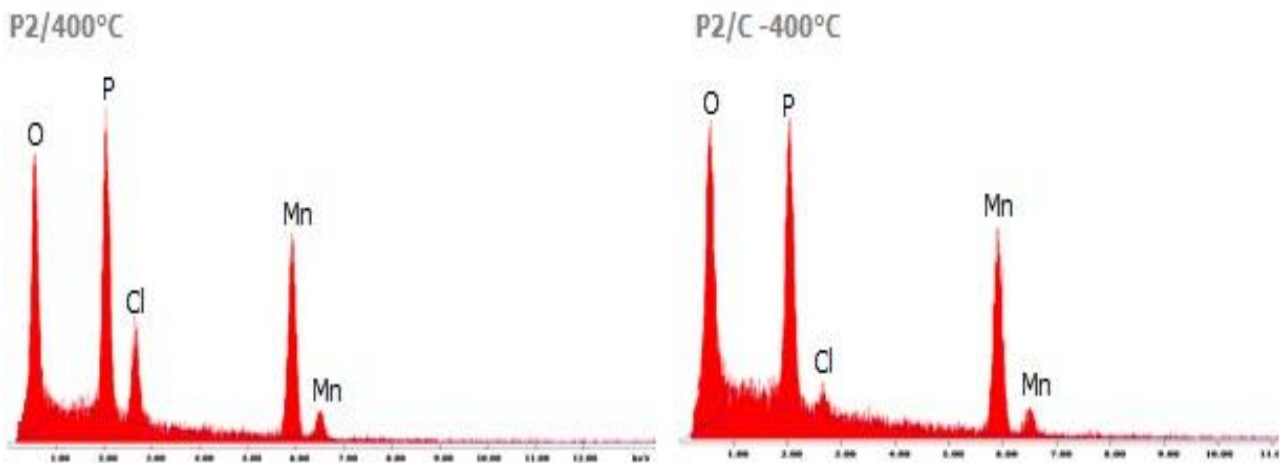
Figure 4 : SEM micrographs of the Product-2 (left) and Product-2/C (right) at 400°C

The EDS results obtained shown in Fig. 5 for the Product-1 and in Fig. 6 for the Product-2, confirm the presence of the Mn, P, O atoms and are consistent to those of the literature, contrariwise the peak of Li is not visible because of its low activation energy.
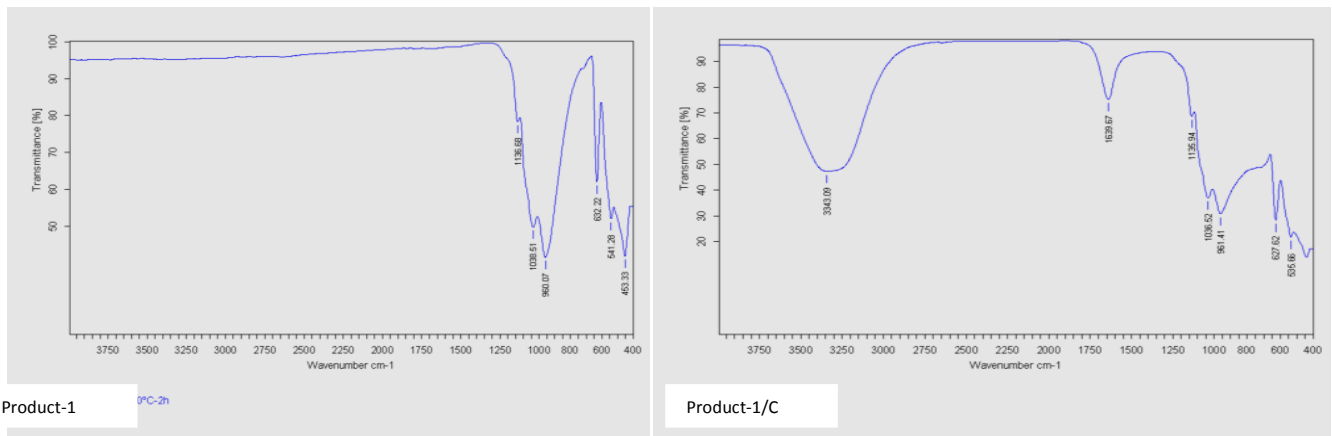

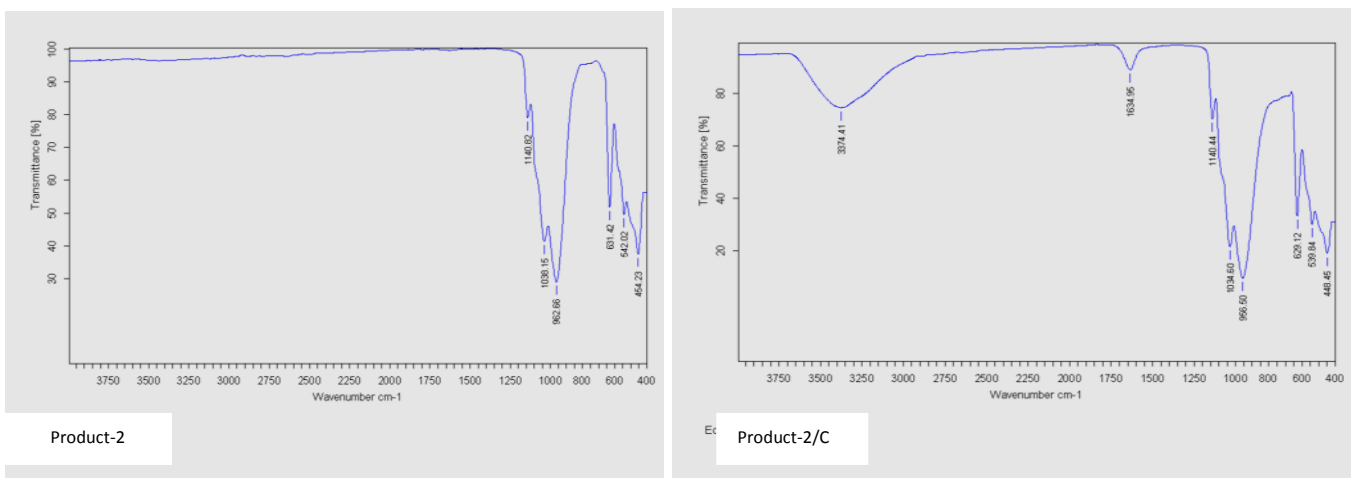**Figure 5 :** EDS measurements of the Product-1 and Product-1/C at 700°C

Figure 6 : EDS measurements of the Product-2 and Product-2/C at 400°C

3.3. Fourier transform infrared spectroscopy (FTIR)

Figures7 &8 show the FTIR spectra of all pure and carbon coated $LiMnPO_4$ nanoparticles. From figure 7, FTIR spectra show bands at ≈ 960 cm^{-1} and ≈ 1038 cm^{-1}, which are due to symmetrical and asymmetrical stretching of PO_4^{-3}. The IR bands between 640 and 450 cm^{-1} are due to the asymmetric bending O–P–O mode. Thus, FTIR results confirmed the presence of PO_4^{-3} structure in the pure and carbon coated $LiMnPO_4$ nanoparticles for the Product-1(at 700°C). Furthermore, carbon coated $LiMnPO_4$ (Product-1/C) nanoparticles sample showed extra bands at 3343cm^{-1} and 1639 cm^{-1}, which are attributed to the stretching frequency of OH (due to the adsorbed moisture) and the symmetrical stretching C-C respectively, and confirmed the presence of carbon over $LiMnPO_4$ nanorods in carbon coated samples.

Figure 7: FTIR spectra of the Product-1 and Product-1/C at 700°C
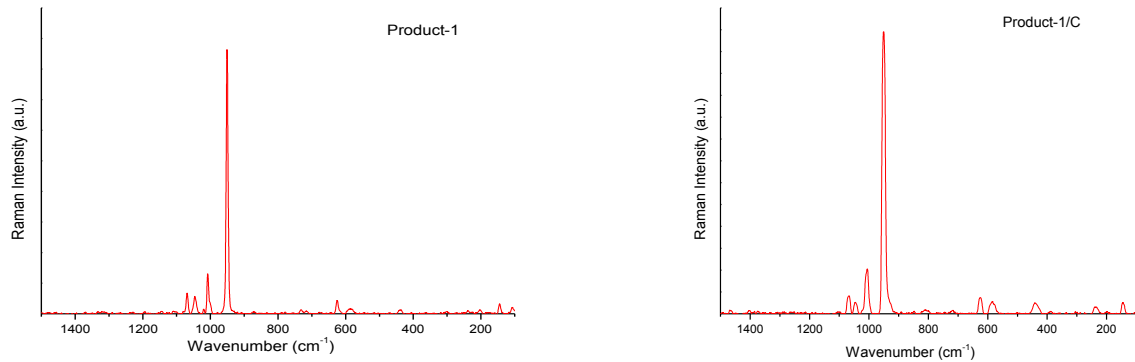

Figure 8: FTIR spectra of the Product-2 and Product-2/C at 400°C
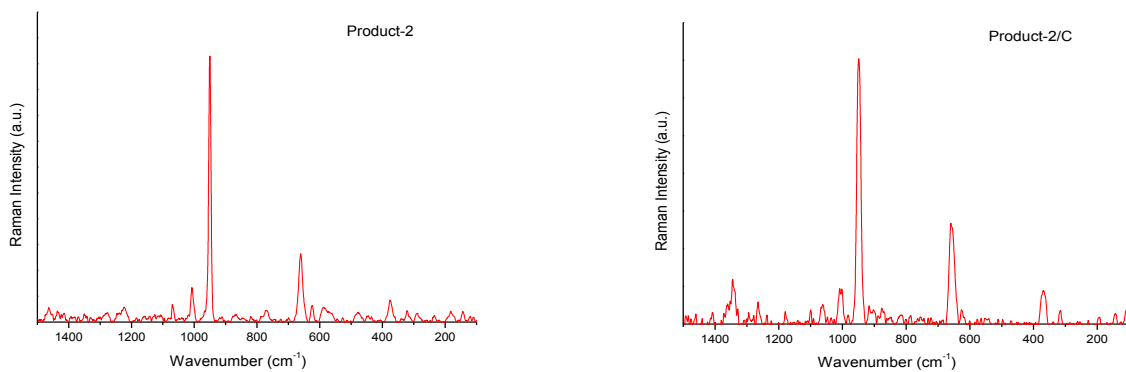
3.4. Raman spectra

For the figure 8, that present the Product-2 and Product-2/C results, it's shown approximately the same peaks position with the above results of Product-1 and Product-1/C with a small difference intensity.

Figures 9&10 show that the products are characterized by a very sharp band at 950 cm^{-1} assigned to the phosphate $PO4^{3-}$ symmetric stretching mode. The Raman bands between 1000 and 1100 cm^{-1} are assigned to the PO_4^{3-} anti-symmetric stretching modes. Two sharp bands at 591 and 627 cm^{-1} (for the Product-1, Product-1/C and Product-2) and one band at 591cm^{-1} (for the Product-2/C) are attributed to the v_4 out of plane bending modes of the PO_4^{3-} units. All bands between 400 and 500 cm^{-1} are assigned to the v_2 PO_4^{3-} bending modes.

J. Mater. Environ. Sci. 7 (1) (2016) 40-49
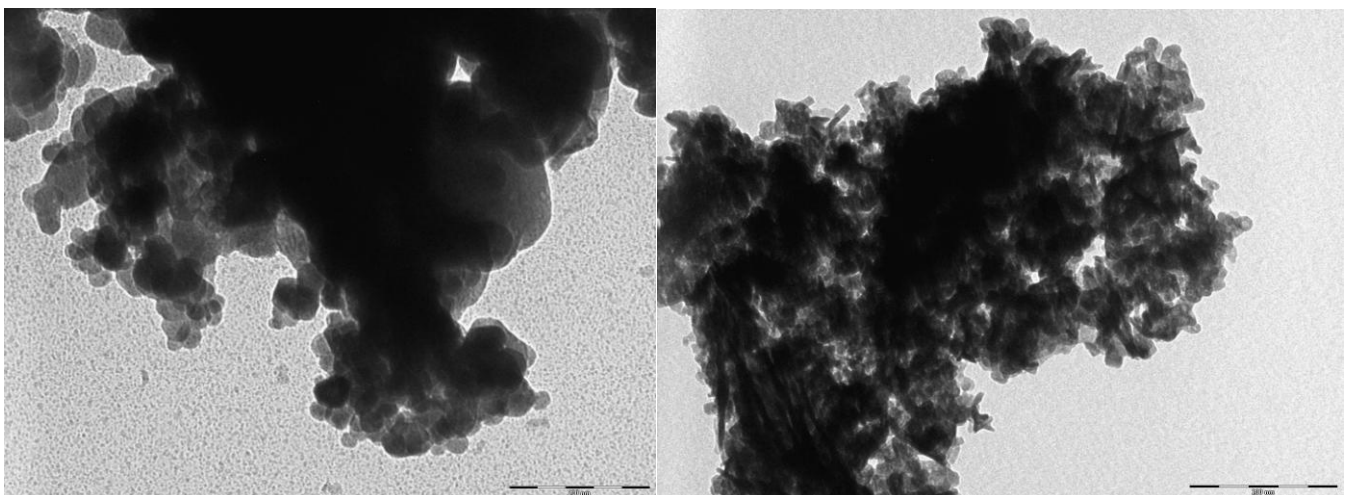*ISSN: 2028-2508*
CODEN: JMESCN

El Khalfaouy et al.

Figure 9: Raman spectrum of Product-1 and Product-1/C

Figure 10: Raman spectrum of Product-2 and Product-2/C

3.5. Transmission electron microscopy (TEM)

As can be seen from TEM micrographs in Figure 11, the samples (Prodcut-1/C and Product-2/C) consist of well-separated particles. The estimated particle size is between 200 nm and 4000 nm. Particles are not very well dispersed in carbon matrix formed during the ball milling process because a small amount of the carbon precursor was used in the synthesis.

Figure 11: TEM images of the carbon coated LiMnPO4, Product-2/C (left) and Product-1/C (right)

So the differences in morphology and dispersity between $LiMnPO_4$ and $LiMnPO_4/C$ powder shown are owing to carbon coating originated from Starch during the annealing process. It is hard to ooze into the precursor for Starch with dense accumulated secondary particles in the Product-1 and Product-2. This leads to non-uniform carbon coating, which affects the electrochemical performance due to its electronic conductivity improved by carbon coating. So the method to obtain homogenous carbon coating needs to be explored in the further investigation.

Conclusion

Nano-crystalline olivine-type $LiMnPO_4$ is prepared at different conditions by combination of precipitation method with solid-state blending. It has been demonstrated that the initial concentration of the precursors (Mn, PO_4) according to the calcination temperature (400 - 700°C) can affect the structure and the morphology of lithium phospho-olivine, which is promising cathode material in lithium ion batteries. Particle growth can be effectively reduced by ball milling process when we prepare the material doped with carbon source $LiMnPO_4/C$.

References

1. Piana M., Arrabito M., Bodoardo S., D'Epifanio A., Satolli D., Croce F., Scrosati B., *J. Ionics.* 8 (2002) 17.
2. Zhou F., Kang K., Maxisch T., Ceder G., Morgan D., *J. Solid State Commun*. 132 (2004) 181.
3. Yamada A., Hosoya M., Chung S.C., Kudo Y., Hinokuma K., Liu K.Y., Nishi Y., *J. Power Sources* 119–121 (2003) 232.
4. Yamada A., Chung S.C., *J. Electrochem Soc*. 148 (2001) A960.
5. Padhi A. K., Nanjundaswamy K. S., Goodenough J. B., *J. Electrochem. Soc.* 144 (1997) 1188.
6. Ravet N., Goodenough J. B., Besner S., Simoneau M., Hovington P., Armand M., *The Electrochemical Society and The Electrochemical Society of Japan Meeting Abstracts,* Abstract 127 (1999) vol. 99-2.
7. Besner S., Choquette Y., Magnan J.F., Allaire F., Vallee A., Potvin E., Hovington P., *The Electrochemical Society and The Electrochemical Society of Japan Meeting Abstracts,* Abstract 204 (1999) Vol. 99-2.
8. Andersson S., Thomas J. O., Kalska B., Haggstrom L., *Electrochem. Solid-State Lett.* 3 (2000) 66.
9. Andersson A. S., Kalska B., Haggstrom L., Thomas J. O., *Solid State Ionics.* 130 (2000) 41.
10. Takahashi M., Tobishima S., Takei K., Sakurai Y., *the Battery Symposium of Japan Extended Abstracts* 347 (2000) 40.
11. Yamada A., Chung S. C., Hinokuma K., *J. Electrochem. Soc*. 148 (2001) A224.
12. Prosini P. P., Zane D., Pasquali M., *Electrochim. Acta* 46 (2001) 3517.
13. Ravet N., Chouinard Y., Magnan J. F., Besner S., Gauthier M., Armand M., *J. Power Sources.* 97-98 (2001) 503.
14. Andersson A. S., Thomas J. O., *J. Power Sources.* 97-98 (2001) 498.
15. Delacourt C., Laffont L., Bouchet R., Wurm C., Leriche J. B., Morcrette M., Tarascon J. M., Masquelier, C., *J. Electrochem. Soc.* 152 (2005) A913.
16. Yamada A., Kudo Y., Liu K. Y., *J. Electrochem. Soc.* 148 (2001) A747.
17. Oh S. M., Oh S. W., Yoon C. S., Scrosati B., Amine K., Sun Y. K., *Adv. Funct. Mater.* 20 (2010) 3260.
18. Delacourt C., Poizot P., Morcrette M., Tarascon J. M., Masquelier C., *Chem. Mater.* 16 (2004) 93.
19. Xiao J., Xu W., Choi D., Zhang J. G., *J. Electrochem. Soc*. 157 (2010) A142.
20. Drezen T., Kwon N. H., Bowen P., Teerlinck I., Isono M., Exnar I., *J. Power Sources*. 174 (2007) 949.
21. Dominko R., Bele M., Gaberscek M., Remskar M., Hanzel D., Goupil J. M., Pejovnik S., Jamnik J., *J. Power Sources*. 153 (2006) 274.
22. Martha S. K., Markovsky B., Grinblat J., Gofer Y., Haik O., Zinigrad E., Aurbach D., Drezen T., Wang D., Deghenghi G., Exnar I., *J. Electrochem. Soc.* 156 (2009) A541.

23. Wang D., Buqa H., Crouzet M., Deghenghi G., Drezen T., Exnar I., Kwon N. H., Miners J. H., Poletto L., Gratzel M., *J. Power Sources 189 (2009) 624.*

24. Li G. , Azuma A., Tohda M., *Electrochem. Solid-State Lett.* 5 (2002) A135.

25. Martha S. K., Grinblat J., Haik O., Zinigrad E., Drezen T., Miners J. H., Exnar I., Kay A., Markovsky B., Aurbach D., *Angew. Chem. Int. Ed*. 48 (2009) 8559.

26. Barpanda P., Djeliab K., Recham N., Armand M., Tarascon J. M., *J. Mater. Chem.* 21 (2011) 10143.

27. Bakenov Z., Taniguchi I*., J. Power Sources*. 195 (2010) 7445.

28. Sronsri C., Noisong P., Danvirutai C*., J. Solid State Sciences* 32 (2014) 67-75.

29. Wang D., Buqa H., Crouzet M., Deghenghi G., Drezen T., Exnar I., Kwon N.H., *J. Power Sources* 189 (2009) 624.

30. Fang H.S., Li L.P., Li G.S., *Chem. Lett*. 36 (2007) 436.

(2016) ; http://www.jmaterenvironsci.com